Earthline Journal of Mathematical Sciences
E-ISSN: 2581-8147
Volume 14, Number 1, 2024, Pages 75-103
https://doi.org/10.34198/ejms.14124.075103

Dual Stratification Effects on Mixed Convective Electro-magnetohydrodynamic Flow over a Stretching Plate with Multiple Slips and Cross Diffusion

Mike Baako[1], Christian John Etwire[2], Golbert Aloliga[3,*] and Yakubu Ibrahim Seini[4]

[1] C. K. Tedam University of Technology and Applied Sciences, P. O. Box 24, Navrongo, Upper East Region, Ghana
e-mail: Baakomike28@gmail.com

[2] C. K. Tedam University of Technology and Applied Sciences, P. O. Box 24, Navrongo, Upper East Region, Ghana
e-mail: jecpapa@yahoo.com

[3] C. K. Tedam University of Technology and Applied Sciences, P. O. Box 24, Navrongo, Upper East Region, Ghana
e-mail: aloligagolbert@gmail.com

[4] School of Engineering, University for Development Studies, Nyankpala Campus, Northern Region, Ghana
e-mail: yakubuseini@yahoo.com

Abstract

This paper analyzed the effects of dual stratification on mixed convective electro-magnetohydrodynamic flow over stretching plates with multiple slips. With the aid of the similarity transformation technique were, the governing boundary equations, that were partial differential equations, were changed to a couple of ordinary differential equations and then solved with fourth order Runge Kutta method and Newton's Raphson shooting techniques. It was observed that the magnetic field, Buoyancy ratio, permeability, momentum slip parameters, Dufour, Soret and Brinkmann numbers made the thermal boundary layer thickness to increase but the solutal stratification, electric field, chemical reaction, solutal slip, suction, thermal slip and thermal stratification parameters, Prandtl, Richardson and Lewis number decreased the thickness of the thermal boundary layer. The Buoyancy ratio, permeability, momentum slip, thermal slip and thermal stratification parameters and Soret number enhanced the solutal boundary layer thickness.

Received: September 14, 2023; Accepted: October 17, 2023; Published: November 4, 2023

2020 Mathematics Subject Classification: 76-10, 76A05, 76D05.

Keywords and phrases: dual stratification, multiple slips, magnetic field, electro-magnetohydrodynamic, cross diffusion.

*Corresponding author

Nomenclature

(x, y) = Cartesian coordinates

(u, v) = Velocity components along x and y axes

A_1, A_2 = Thermal stratification coefficients

B_1, B_2 = Solutal stratification coefficients

T_∞ = Free-stream temperature of fluid

T_w = Temperature of the sheet

T = Temperature of fluid

c_p = Specific heat at constant pressure

k' = Permeability of the porous media

K = Permeability parameter

D_m = Mean diffusion coefficient

k_t = Thermal-diffusion ratio

c_s = Concentration susceptibility of the fluid

S_o = Soret number

g = Acceleration due to gravity

q_1 = Velocity slip parameter

q_2 = Temperature slip coefficient

q_3 = Concentration slip coefficient

Q_3 = Solutal slip parameter

D_0 = Dufour number

Le = Lewis number

N_B = Buoyancy ratio parameter

q_m = Wall mass flux

h_f = Heat transfer coefficient

Pr = Prandtl number

C_f = skin-friction coefficient

Re = Reynolds number

Nu = Nusselt number

q_w = Wall heat flux

Br = Brinkman number

U_∞ = Free stream velocity of fluid

S = Suction parameter

C = Concentration of fluid

C_∞ = Free-stream concentration of fluid

C_w = Concentration of the sheet

D = Diffusion coefficient

T_m = Mean temperature of the fluid

Sh = Sherwood number

S_s = Solutal stratification parameter

S_T = Thermal stratification parameter

R_i = Richardson number

M = Magnetic field parameter

E = Electric field parameter

S = Suction parameter

Q_1 = Momentum slip parameter

Q_2 = Thermal slip parameter

Symbols

η = Dimensionless Variable	θ = Dimensionless Temperature
τ_w = Wall shear stress	γ = Reaction rate parameter
υ = Kinematic viscosity of fluid	φ = Dimensionless concentration
ρ = Density of fluid	α_v = Viscoelastic parameter
α = Thermal diffusivity of fluid	β = Chemical reaction rate parameter
ρ_∞ = Ambient density of the fluid	ρ_p = Density of the fluid particles
	ψ = Stream function

1. Introduction

The study of stratification effects on electro-magnetohydrodynamics continues to physically run simultaneously with heat and mass transport, thus it is worth looking into the two fold stratification mechanism (thermal and mass stratifications) on fluids Hayat *et al.* [1]. Stratification of magnetohydrodynamic flow on fluids has received must attention in recent years. The effect of free convective MHD flow in a micropolar fluid with double stratification is an important component in fluid Srinivasacharya and Upendar [2]. Electro-magnetohydrodynamic micropumps in a spatially non-uniform magnetic field revealed that, when the decay factor of the magnetic field increases, the EMHD velocity drops. Aside from that, EMHD velocity rises as the electric field strength rises Jian and Chang [3]. The influence of temperature on stratification of MHD nanofluid radiative flow in a nonlinear stretching sheet with varying thickness was found to improve fluid temperature, velocity and fraction of the volume of nanoparticle concentration Yahaya and Faisal [4]. Thermally mixed convective flow of stratified MHD nanofluid across a viscous dissipation effect on an increasingly stretched surface showed that, as the thermal stratified parameter is increased, the temperature and concentration profiles are lowered Besthapy *et al*. [5]. Effects of twofold stratification on mass and heat transfer in a non-uniform MHD nanofluid flow across a flat surface with shooting technique, they used the Runge-Kutta-Fehlberg fourth order algorithm. Thermal stratification reduced temperature of the fluid, while solutal stratification reduced nanoparticle concentration, according to the findings Mutuku and Makinde [6]. Modeling non-Fourier energy for investigating double stratified nanofluid flow past a permeable shrinking/stretching surface. The implementation of the solutal and thermal stratification parameters resulted in a small increase in temperature and concentration Khashi'ie *et al*. [7].

Reddy and Chamkha [8] analysed the implications of the Dufour and Soret numbers in unstable MHD mass and heat transport with thermophoresis and non-uniform heat generating absorption from permeable stretched. Increasing Soret number or reducing Dufour number reduces skin friction and mode of heat for shrinking sheets, whereas the opposite is true for stretching sheets Dulal *et al*. [9]. The impact of Ohmic heat on Casson fluid MHD mixed convection flow using the Range-Kutta-Fehlberg method was studied by Gireesha *et al*. [10]. Impacts of Dufour and Soret over mass and heat transfer pattern of the disrupted flow component causes lack of originality in a presented wave-like tendency in the y-axis, as revealed by Gbadeyan *et al*. [11]. Raddy *et al*. [12] employed the Homotopy analysis evaluate the Dufour and Soret effect over MHD viscoelastic fluid flows through an infinite vertically stretching sheet. Rasool *et al*. [13] revealed that the Soret and Dufour numbers have different features in fluid Significants of Dufour and Soret numbers on binary chemical reaction and thermal radiation on Darcy Forchheimer nanofluids flow is a key that influences the raising effect of both temperature and concentration. The Dufour and Soret's influence on forced convection flow involving Buongiorno's nanofluid theory toward a moving item needle resulted that as the needle thickness increases, the solution mass and heat percentages transfer mode decreased Salleh *et al*. [14]. MHD mixed convection nanofluid flow over a nonlinear has been convectively heated due to the Soret effect on an extended surface which causes a rise of values of Soret number with rising magnetic field values decreasing the speed distribution Bouslimi *et al*. [15].

MHD slip flow for viscoelastic fluid across the stretched sheet has numerous solutions for mass and heat transfer Turkyilmazoglu [16]. Daniel *et al*. [17] examined the MHD nanofluid flow through permeable nonlinear stretching/shrinking sheet, the impact of slip and convective circumstances, was that heat and mass convective boundary conditions augmented temperature of nanoparticle concentration field. The numerous slip effects on MHD axisymmetric buoyant nanofluid flow with chemical reaction and radiation over a stretching sheet indicated that, in terms of numerous slip effects, boundary layers rise, whiles the influence of thermal slip on Nusselt number grows as values rise Khan *et al*. [18]. The impact of multiple slips on MHD unstable viscoelastic nanofluid flow with radiation across a permeable stretched sheet shows that the boundary layers expand when multiple slips are present. The velocity distribution was also controlled by the viscoelastic and buoyancy parameters, and it decreased as the magnetic parameter was increased Khan *et al*. [19]. The influence of numerous slip on unsteady MHD flow mass and heat transfer infringing on a porous stretched sheet with radiation

was realised that the skin fraction coefficient rises as magnetic field, Prandlt, Schmidt numbers, uncertainty parameter, and suction parameter increase Mabood and Shateyi [20]. Analytical investigation into the MHD slip transfer of heat with viscous dissipation and thermal radiation of Darcy flow of viscoelastic fluid across a stretching sheet is a key factor that, increases numbers of porosity, magnetic, velocity slip, thermal radiation parameters and Eckert number causing the temperature field to increase Wahid *et al*. [21]. A studied on non-Newtonian slippery Nanofluid flow caused by a stretching sheet across a porous medium with heat generation and thermal slip was carried out by Abass *et al*. [22]. The thermal slip parameter and the mixed convection parameter are demonstrated to have a significant impact on the wall heat transfer coefficient. Ibrahim and Gizewu [23] investigated the three-dimensional continuous thin film flow of tangent hyperbolic fluid past a stretching surface together with nonlinear mixed convection flow and entropy production. As shown in works by Yin *et al*. [24], the literature survey reveals a number of research that explore the viability of obtaining exact solutions for specific nonlinear models. There was another report on MHD free convective stagnation-point flow toward an inclined nonlinearly stretching sheet embedded in a porous medium Biswal *et al.* [25]. The non-Newtonian has been the subject of investigation since Sher Akbar and Mllawi [26] investigated the slip velocity of a non-Newtonian fluid moving above a continuously stretched surface employing double-diffusive nanofluid. The heat transfer properties of a typical non-Newtonian Oldroyd-B fluid are significantly influenced by the salt concentration and the presence of nanoparticles. In recent years, Shehzad *et al*. [27] released their investigation of MHD non-Newtonian fluid flow via an inclined permeable and rotating plate. A numerical analysis in order to comprehend the two-dimensional flow behavior of power-law fluids through a rotating elliptic cylinder in an unconfined domain. The findings of this study unequivocally demonstrate that the flow phenomenon around a rotating elliptic cylinder strongly depends on the power-law index, rotational speed, aspect ratio, and Reynolds number Kumar and Sahu [28].

It is evident from the literature survey that investigations into stratification effect on MHD mixed convective flow with induced electric field over slippery plate is limited. The research sought to investigate the effects of dual stratification on mixed convective electro-magnetohydrodynamic flow over a stretching plate with multiple slip.

2. Mathematical Formulation

Consider a steady, laminar, incompressible, two-dimensional mixed convective flow of an electrical conducting and stratified fluid past a stretching surface embedded in

porous media with Soret and Dufour effects and multiple slips. External transverse magnetic and electric fields of intensity B_0 and E_0 respectively are applied to the flow. The induction due to the magnetic field and hall current effects are disregarded for very small magnetic Reynolds number. The x-axis is parallel to the stretching sheet, and the y-axis is perpendicular to it. The stretching plate's velocity is assumed to be proportional to its distance from the origin (that is $u_w = bx$). The stretching sheet's temperature and concentration are $T_w = T_0 + A_1 x$ and $C_w = C_0 + B_1 x$ respectively whereas the fluid's ambient concentration and temperature are $C_\infty = C_0 + B_2 x$ and $T_\infty = T_0 + A_2 x$ respectively.

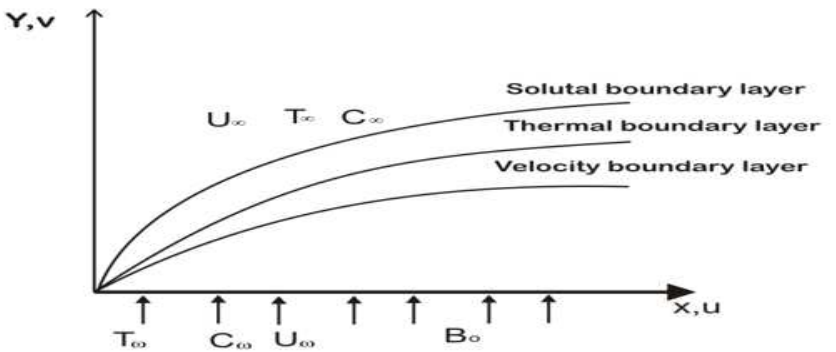

Figure 1: Schematic diagram of the flow.

By the boundary layer approximations, the continuity, momentum, energy and concentration equations modelling the flow problem can be expressed as:

$$\frac{\partial u}{\partial x} + \frac{\partial v}{\partial y} = 0, \tag{1}$$

$$u\frac{\partial u}{\partial x} + v\frac{\partial u}{\partial y} = \upsilon\frac{\partial^2 u}{\partial y^2} - \frac{\sigma B_0}{\rho}(B_0 u - E_0) - \frac{\upsilon}{k'}u + \frac{1}{\rho}\left[\rho_\infty \beta g(1 - C_\infty)(T - T_\infty) - g\left(\rho_p - \rho_\infty\right)(C - C_\infty)\right], \tag{2}$$

$$u\frac{\partial T}{\partial x} + v\frac{\partial T}{\partial y} = \alpha\frac{\partial^2 T}{\partial y^2} + \frac{\mu}{\rho c_p}\left(\frac{\partial u}{\partial y}\right)^2 + \frac{\sigma}{\rho c_p}(B_0 u - E)^2 + \frac{D_m k_t}{c_s c_p}\frac{\partial^2 C}{\partial y^2}, \tag{3}$$

$$u\frac{\partial C}{\partial x} + v\frac{\partial C}{\partial y} = D\frac{\partial^2 C}{\partial y^2} - \gamma(C - C_\infty) + \frac{D_m k_t}{T_m}\frac{\partial^2 T}{\partial y^2}, \tag{4}$$

subject to the boundary conditions;

$$u(x,0) = bx + q_1\frac{\partial u}{\partial y},\ \ v(x,0) = -v_w,\ \ T(x,0) = T_0 + A_1 x + q_2\frac{\partial T}{\partial y},\ \ C(x,0) = C_0 +$$

$B_1 x + q_3 \frac{\partial C}{\partial y}$, at $y = 0$

$u(x,\infty) \to 0,\ T(x,\infty) \to T_0 + A_2 x,\ C(x,\infty) \to C_0 + B_2 x,$ as $y \to \infty$. (5)

3. Similarity Transformations

Equation (1) is satisfied identically by defining the stream function, $\psi(x,y)$ as;

$$u = \frac{\partial \psi}{\partial y} \text{ and } v = -\frac{\partial \psi}{\partial x}. \tag{6}$$

The following independent variable η, dimensionless temperature $\theta(\eta)$, stream function $\psi(x,y)$, and dimensionless concentration $\phi(\eta)$ were used to convert to the flow equations into nonlinear ordinary differential equations (Goyal and Bhargava [29]);

$$\eta = y\sqrt{\frac{b}{\upsilon}},\ \psi(x,y) = \sqrt{b\upsilon}xf(\eta),\ \theta(\eta) = \frac{T-T_\infty}{T_w-T_0},\ \phi(\eta) = \frac{C-C_\infty}{C_w-C_0}. \tag{7}$$

Plugging equations (6) and (7) into equations (2) to (5) yield;

$$f'''(\eta) + f(\eta)f''(\eta) - f'^2(\eta) - M\left(f'(\eta) - E\right) - Kf'(\eta) + R_1\left(\theta(\eta) - N_B\phi(\eta)\right) = 0,$$

$$\theta''(\eta) + Pr\, f'(\eta)(\theta(\eta) + S_T) + Pr\, f(\eta)\theta'(\eta) + Brf''^2(\eta) + BrM\left(f'(\eta) - E\right)^2 + Pr\, D_0\, \phi''(\eta) = 0,$$

$$\varphi''(\eta) - Pr\, L\, ef'(\eta)[\varphi(\eta) + S_s] + Pr\, L\, ef(\eta)\varphi'(\eta) - Pr\, L\, e\beta\varphi(\eta) + Pr\, L\, eS_0\theta''(\eta) = 0, \tag{8}$$

subject to the boundary conditions:

$$f'(0) = 1 + Q_1 f''(0),\ f(0) = S,\ \theta(0) = 1 - S_T + Q_2\theta'(0),\ \phi(0) = 1 - S_s + Q_3\varphi'(0),\ f'(\infty) \to 0,\ \theta(\infty) \to 0,\ \phi(\infty) \to 0, \tag{9}$$

where $M = \frac{\sigma B_0^2}{\rho b}$, $R_1 = \frac{Gr}{Re^2}$, $E = \frac{E_0}{B_0 bx}$, $K = \frac{\upsilon}{k'b}$, $G_T = \frac{\beta_T(1-C_\infty)(T_w-T_0)x^2}{\rho\upsilon^2}$, $N_B = \frac{(\rho_p-\rho_\infty)(C_w-C_0)}{\rho_\infty\beta(C-C_\infty)(T_\infty-T_0)}$, $Pr = \frac{\upsilon}{\alpha}$, $S_T = \frac{A_2}{A_1}$, $Br = \frac{\mu u_w^2}{k(T_w-T_0)}$, $E = \frac{E_0}{B_0 bx}$, $\frac{D_m K_t(C_w-C_0)}{C_s C_p \upsilon(T_w-T_0)} = D_0$, $Le = \frac{\alpha}{D}$, $S_s = \frac{B_2}{B_1}$, $\beta = \frac{\gamma}{b}$, $S_0 = \frac{D_m k_t(T_w-T_0)}{\upsilon T_m(C_w-C_0)}$.

The skin-friction coefficient (C_f), Nusselt number (*Nu*), and Sherwood number (*Sh*) are the main parameters of engineering relevance. They are defined respectively as;

$$C_f = \frac{\tau_w}{\rho u_w^2},\ Nu = \frac{xq_w}{k(T_w-T_0)},\ Sh = \frac{xq_m}{D(C_w-C_0)}, \tag{10}$$

where τ_w represents wall shear stress, q_w represents wall heat flux and q_m represents wall mass flux, which are expressed respectively as:

$$\tau_w = \mu \frac{\partial u}{\partial y}\Big|_{y=0}, \; q_w = -k \frac{\partial T}{\partial y}\Big|_{y=0}, \; q_m = -D \frac{\partial C}{\partial y}\Big|_{y=0}. \tag{11}$$

Plugging equation (11) into (10) gives,

$$Re_x^{1/2} C_f = f''(0), \tag{12}$$

$$Re_x^{-1/2} Nu = -\theta'(0), \tag{13}$$

$$Re_x^{-1/2} Sh = -\varphi'(0) \tag{14}$$

where $Re_x = \frac{u_w x}{\upsilon}$ is the local Reynolds number. The coupled nonlinear differential equations were solved numerically by employing the fourth order Runge-Kutta algorithm with a shooting method.

4. Results and Discussion

The results of the current model for Nusselt number represented by $(-\theta'(0))$ was compared to works by Wang [30] and Goyal and Sidawi [31] for different values of the Prandtl number (Pr) and for $S_s = S_T = E = R_i = M = \beta = Q_1 = Q_2 = Q_3 = D_0 = S = Le = Br = K = S_o = N_B = 0$ and their findings were completely in agreement. This verifies the current model. Table 1 illustrates the comparison.

Table 1: Computations showing comparison with Wang [30] and Goyal and Sidawi [31].

	Wang [30]	Goyal and Sidawi [31]	Present Work
Pr	$-\theta'(0)$	$-\theta'(0)$	$-\theta'(0)$
0.7	0.4539	0.4539	0.4539
2.0	0.9114	0.9113	0.9114
7.0	1.8954	1.8954	1.8954
20.0	3.3539	3.3539	3.3539

4.1. Impact of thermophysical parameters on coefficient of skin friction, Nusselt number and Sherwood number

The influence of the thermophysical variables on the skin friction coefficient $\left(f''(0)\right)$, Nusselt number depicted by heat transfer rate $(-\theta'(0))$ and Sherwood number depicted by the mass transfer rate $(-\varphi'(0))$ are illustrated in Table 2 and Table 3. The

skin friction coefficient, Sherwood number and Nusselt number all rise as the Prandtl number and Suction parameter are increased. Also, the electric field parameter and Richardson number are noted to appreciate the Nusselt and Sherwood numbers but lowered the skin friction coefficient. It is also worth noting that as the Soret number rises, the Nusselt number and skin friction coefficient also appreciate as well, while the Sherwood number decays. Furthermore, increasing the permeability, magnetic field, buoyancy ratio, and thermal stratification parameters raise the skin friction coefficient while lowering Sherwood and Nusselt numbers. In addition, the Lewis number, Dufour number, chemical reaction parameter, and Brinkmann number lowered Nusselt number and skin friction coefficient while raising the Sherwood number. Furthermore, hike in the Solutal stratification and solutal slip parameters increase the Nusselt number while lowering the Sherwood number and skin friction coefficient. In addition, raising the thermal slip parameter raises the Sherwood number and skin friction coefficient while lowering Nusselt number. Finally, Nusselt number, Sherwood number and skin friction coefficient are all reduced when the momentum slip parameter is increased.

Table 2: Computational results for $(-f''(0))$, $(-\theta'(0))$ and $(-\varphi'(0))$ for different parameter values, where $R_1, N_B, M, E, Br, S, K = 0.1$ and $Pr = 0.7$.

S_S	Le	S_0	β	S_T	Q_1	Q_2	Q_3	D_0	$-f''(0)$	$-\theta'(0)$	$-\phi'(0)$
0.1	0.3	0.1	0.1	0.1	0.2	0.2	0.2	0.2	0.833359	0.586393	0.318423
0.3									0.832196	0.589044	0.278211
0.5									0.831033	0.591682	0.238011
0.7									0.829869	0.594308	0.197823
	0.5								0.832021	0.576675	0.434588
	0.7								0.831127	0.568117	0.531060
	0.9								0.830483	0.560413	0.613818
		1.0							0.834165	0.593431	0.237883
		2.0							0.835076	0.601571	0.145419
		3.0							0.836003	0.610073	0.049619
			1.0						0.831403	0.572087	0.491060

			2.0						0.830511	0.561293	0.606547
			3.0						0.829962	0.552645	0.693908
				0.3					0.845368	0.527197	0.315197
				0.5					0.857359	0.466667	0.311935
				0.7					0.869311	0.404696	0.308657
					1.0				0.445573	0.512865	0.282941
					3.0				0.213625	0.443570	0.254813
					5.0				0.141720	0.415254	0.244232
						1.0			0.845334	0.381362	0.318975
						2.0			0.852258	0.265883	0.319207
						3.0			0.856014	0.204208	0.319305

Table 3: Computational results for $\left(-f''(0)\right)$, $(-\theta'(0))$ and $(-\phi'(0))$ for different parameter values where $S_S, S_0, \beta, S_T, Q_1 = 0.1, Q_2, Q_3, D_0 = 0.2$ and $Le = 0.3$

R_1	N_B	M	E	Pr	Br	S	K	$-f''(0)$	$-\theta'(0)$	$-\phi'(0)$
0.1	0.1	0.1	0.1	0.7	0.1	0.1	0.1	0.833359	0.586393	0.318423
1.0								0.600577	0.651496	0.351211
2.0								0.383422	0.694503	0.374036
3.0								0.188093	0.725771	0.391583
	1.0							0.884196	0.549776	0.298686
	1.3							0.903194	0.530189	0.289249
	2.0							0.951203	0.431920	0.257856
		0.5						0.920096	0.567445	0.315490
		1.0						1.016257	0.540750	0.307592
		1.5						1.099263	0.517565	0.300381

			0.4					0.801512	0.614273	0.337443
			0.7					0.771467	0.630867	0.351925
			1.0					0.742774	0.640699	0.363818
				1.0				0.838604	0.714526	0.389399
				1.5				0.843629	0.876522	0.488156
				2.0				0.846577	0.999039	0.569224
					1.0			0.827019	0.367164	0.324586
					2.0			0.820231	0.130535	0.331168
					3.0			0.813679	-0.099375	0.337503
						0.5		0.971689	0.670235	0.336828
						1.0		1.161932	0.790281	0.366795
						1.5		1.360541	0.921998	0.405242
							1.0	1.071622	0.497844	0.278800
							2.0	1.258928	0.432354	0.255085
							3.0	1.404032	0.385191	0.239956

4.2. Graphical results

4.2.1. Velocity graphs

In Figure 2 increasing values of solutal stratification parameter increases the thermal diffusion rate thereby reducing fluid's viscosity, leading to the increase in velocity as indicated on the velocity profile. The influence of magnetic field parameter on velocity is seen in Figure 3. The Lorentz force of attraction increases as the thickness of the momentum boundary layer grows for high magnetic field parameter values, yet the velocity increases as a result of the high kinetic energy in the fluid due to the high presence of the thermal diffusion rate. The influence of the Richardson number on velocity profile is shown in Figure 4. The momentum boundary layer thickness grows as the Richardson number increases, resulting in decreasing shear stress on the sheet. This is owing to the fact that when the Richardson number rises, the natural convection effect

increases, which is accompanied by a reduction in the velocity gradient. Figure 5 show that a higher electric field value increases fluid velocity. This is because; the electric field operates as an accelerating force. The Lorentz force becomes stronger as electric field parameter increases, creating more enhancement and resolving sticky effects caused by fluid particles that imply an increase in the thickness of the momentum boundary layer. Excitation in fluid molecules causes a rise in velocity when the electric field parameter is increased. Figure 6 displays effect of Dufour number on the velocity profile. Because the unit mass enthalpy of the mixture decreases as the Dufour number rises, the velocity rises as well. Figure 7 depicts the effect of the Buoyancy ratio parameter on fluid velocity. It has been noticed that when the Buoyancy ratio is high, the fluid velocity decreases making the momentum boundary layer narrower. The velocity decreases in Figure 8 as the Prandtl number rises. This is as a result of the fact that Prandtl number depicts the ratio between momentum and thermal diffusivity. The thermal diffusivity minimizes when Prandtl number values are large due to which temperature decreases and hence reducing the thickness of the momentum boundary layer. When suction parameter is increased, the momentum barrier layer becomes thinner, as shown in Figure 9. This is due to a reduction in fluid velocity as a result of increased suction at the stretched surface. The thermal slip parameter on the velocity graph is displayed in Figure 10. When thermal slip parameter is increased, the temperature drops, and less amount of heat is transported from the plate to the fluid, resulting in a thinner momentum barrier layer.

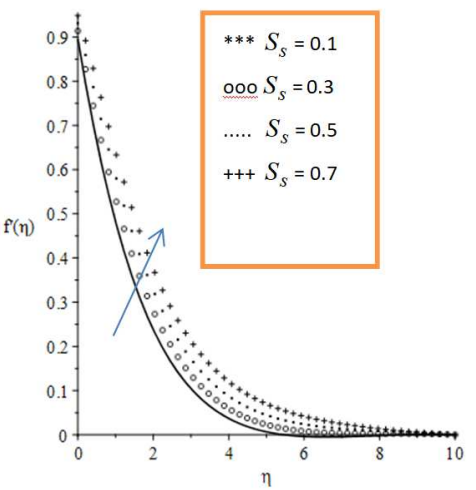

Figure 2: Velocity graph for various values of solutal stratification parameter.

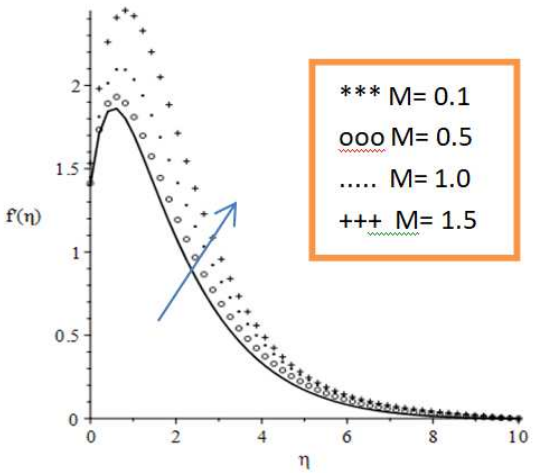

Figure 3: Velocity graph for various values of magnetic field parameter.

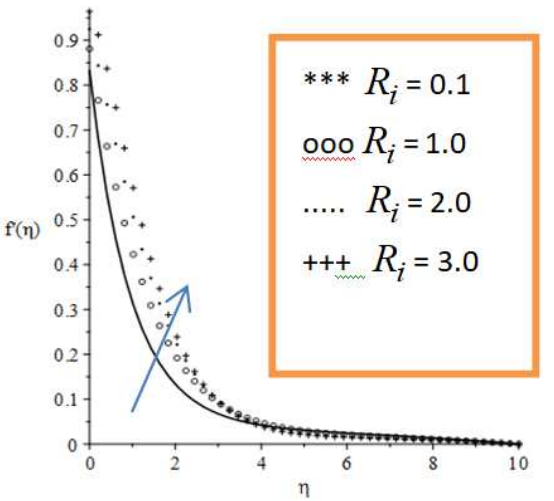

Figure 4: Velocity graph for various values of Richardson number.

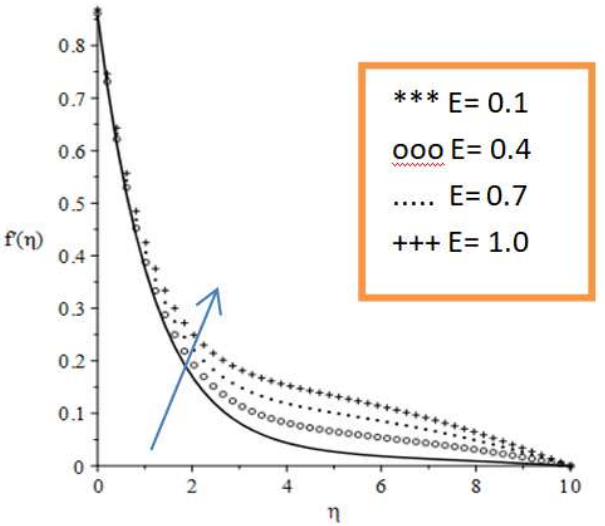

Figure 5: Velocity graph for various values of electric field parameter.

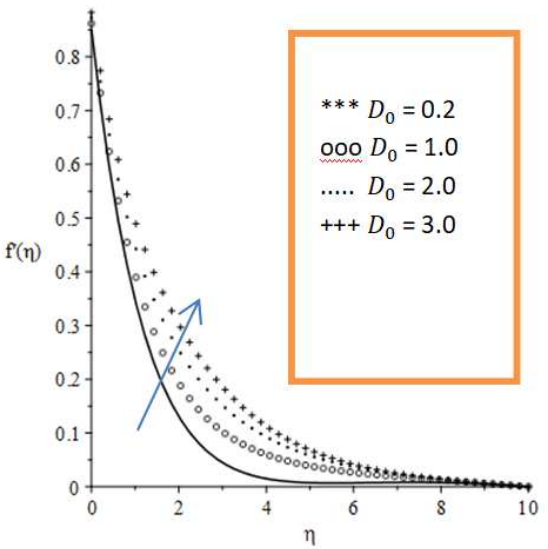

Figure 6: Velocity graph for various values of Dufour numb.

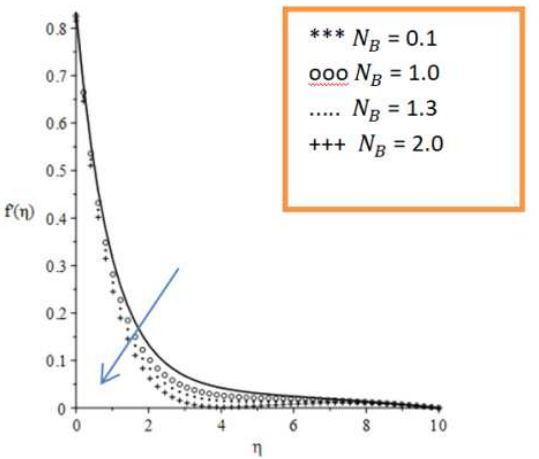

Figure 7: Velocity graph for various values of Buoyancy ratio parameter.

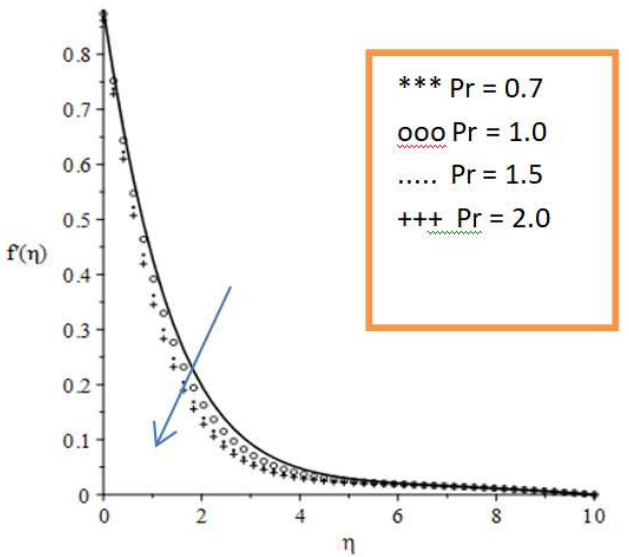

Figure 8: Velocity graph for various values of Prandtl number.

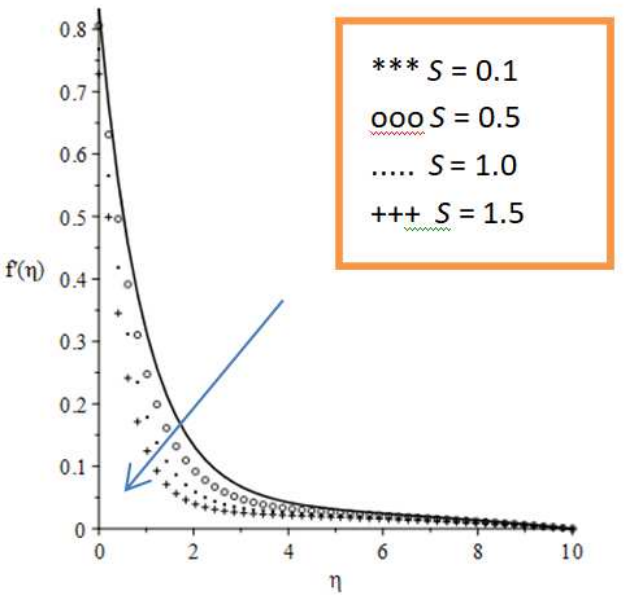

Figure 9: Velocity graph for various values of Suction parameter.

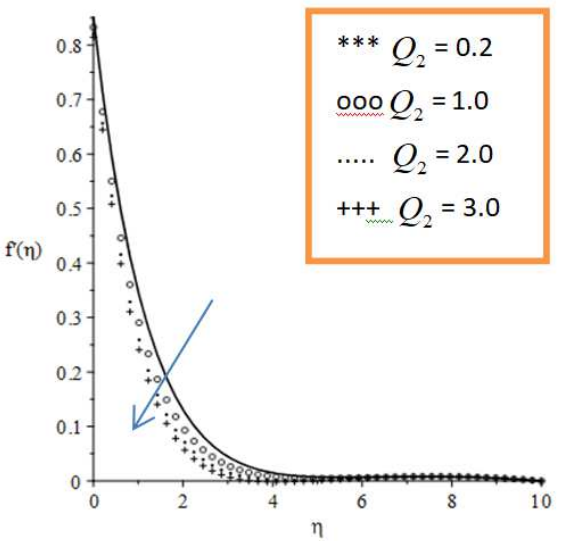

Figure 10: Velocity graph for various values of Thermal slip parameter.

4.2.2. Temperature graphs

The impact of magnetic field parameter on the temperature profile is illustrated in Figure 11. Due to the Lorentz force of attraction, the magnetic field increases the fluid temperature which intends increase thermal boundary layer thickness. Figure 12 shows that, when the Dufour number is increased, the thickness of the thermal boundary layer increases. This is due to the fact that, Dufour number represents the contribution of concentration gradients to the flow's thermal energy flux, which raises the temperature. It is shown in Figure 13 that as the Brinkman number rises, so does the temperature. Because higher Brinkman numbers impede heat transport and this thickens the thermal boundary layer, resulting in larger temperature spikes. Temperature distribution of Soret number is depicted in Figure 14. As the number of Sorets increases, the temperature at the sheet's surface rises slightly. Figure 15 depicts the influence of Prandtl number on the temperature profile. As Prandtl number rises, the thickness of the thermal boundary layer decreases. Thermal diffusivity is decreased and temperature drops when Prandtl number is large. Figure 16 exhibits the temperature profile when the suction parameter is increased. The thermal boundary layer thickness decreases due to closeness of the fluid at the plate surface. The temperature profile for the Lewis number is depicted in Figure 17. The ratio of heat diffusivity to mass diffusivity is known as the Lewis number. In this situation, the thermal barrier thickens as the Lewis number rises, but the rate of heat transfer lowers the temperature due to heat dissipation, which means energy is lost and the temperature falls. Figure 18 shows the temperature profile with different values of thermal stratification parameter. For higher values of the thermal stratification parameter, the fluid temperature drops. When there is a lot of thermal stratification, the difference between the surface and ambient temperatures is physically reduced. As a result, the fluid temperature in the boundary region drops, and the thickness of the thermal boundary layer decreases.

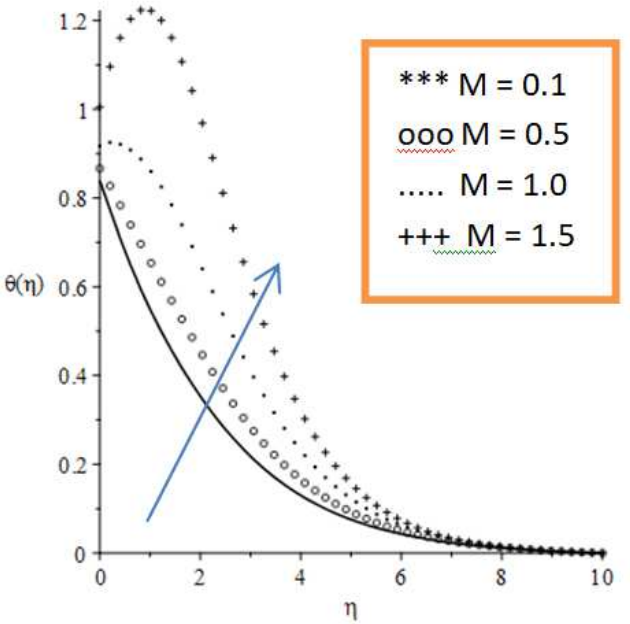

Figure 11: Temperature graph for various values of magnetic field parameter.

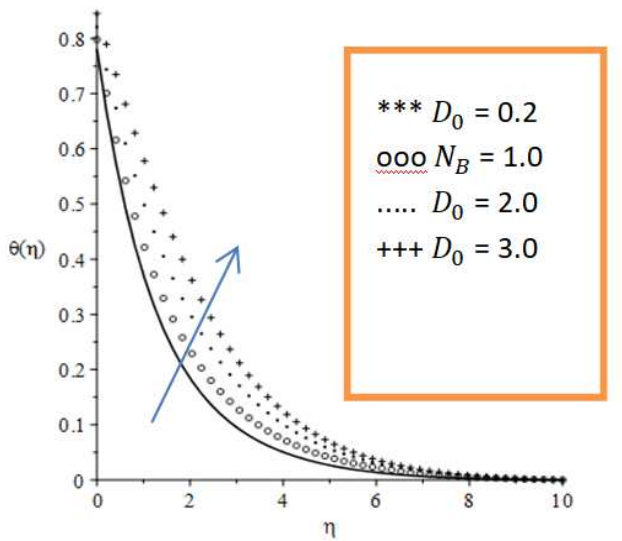

Figure 12: Temperature graph for various values of Dufour number.

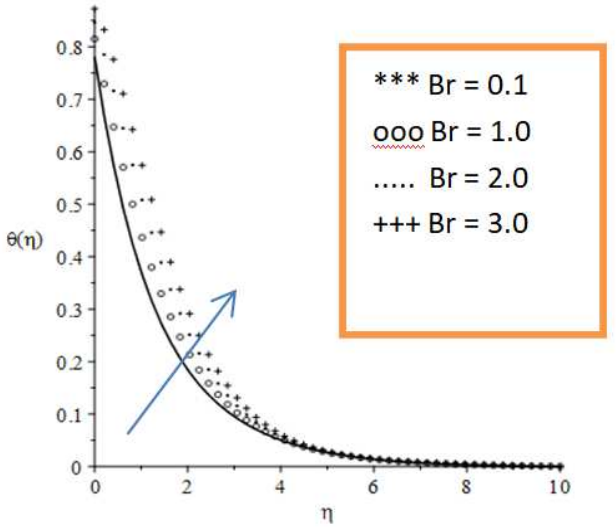

Figure 13: Temperature graph for various values of Brinkmann number.

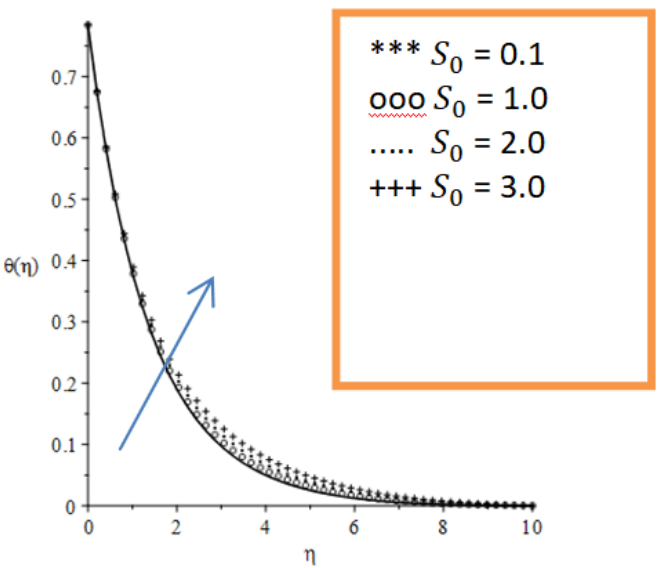

Figure 14: Temperature graph for various values of Soret number values.

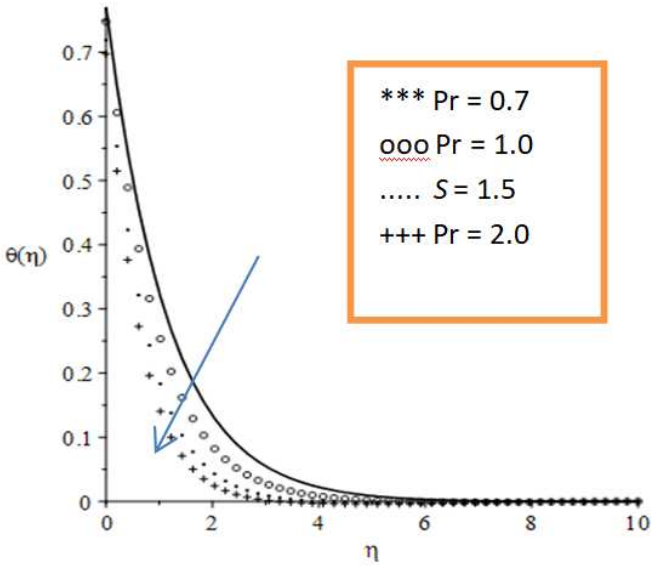

Figure 15: Temperature graph for various values of Prandtl number.

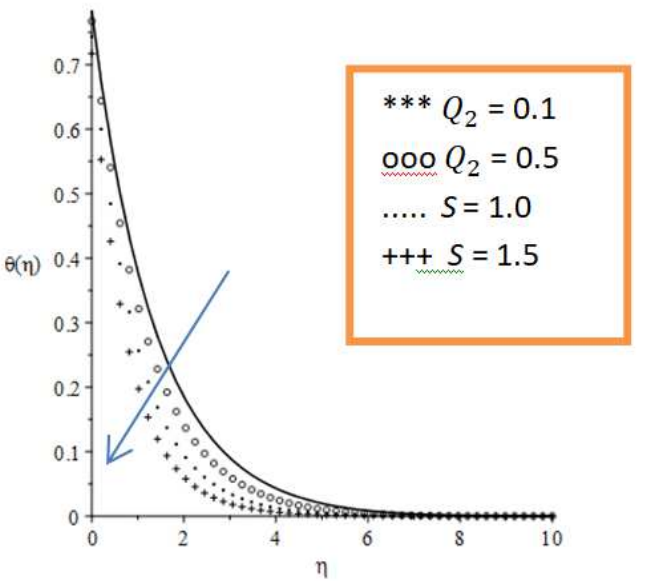

Figure 16: Temperature graph for various values of Suction parameter.

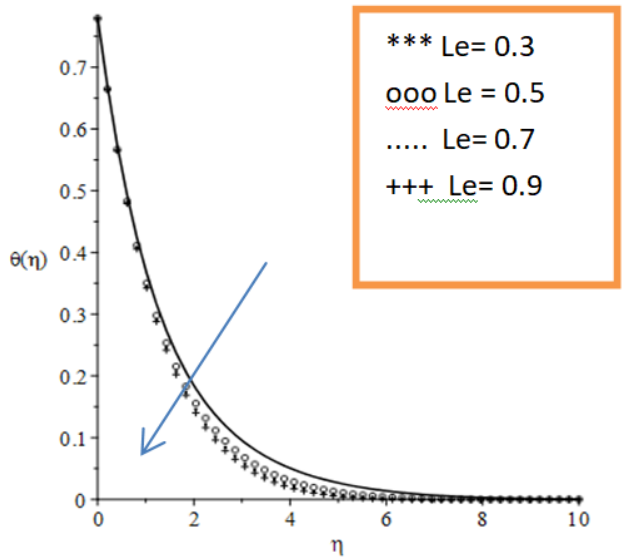

Figure 17: Temperature graph for various values of Lewis number.

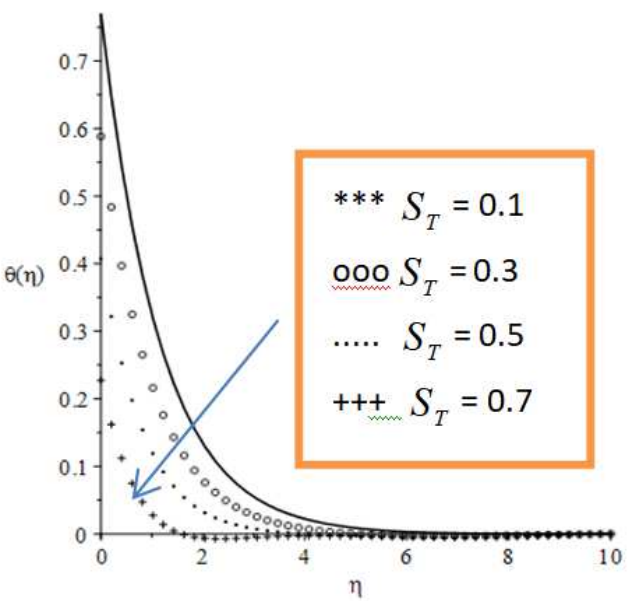

Figure 18: Temperature graph for various values of thermal stratification parameter.

4.2.3. Concentration graphs

The effect of Soret number on the concentration profile is demonstrated in Figure 19. When Soret number is increased, the concentration profile within the flow regime changes dramatically. Figure 20 demonstrates that, an increase in thermal stratification reduces the velocity of the particles. This is because there is reduction of heat in the particles and the velocity drops as a result, thickening the concentration boundary layer. Figure 21 shows how the Prandtl number affects the concentration profile. The Prandtl number reduces the temperature when is increased. This is because as the Prandtl number rises, fluid's thermal conductivity falls, reducing the thickness of the concentration boundary layer. In addition, increasing the magnetic field value lowers the concentration profile as shown in Figure 22. The Lorentz force is a resistive force that slows the velocity of an electrically conducting fluid when the magnetic field parameter is changed. As a result, the concentration of the fluid drops, reducing the thickness of the concentration boundary layer. Figure 23 indicates that increasing the solutal slip parameter reduces concentration by increasing the rate of reaction, which lowers the fluid concentration. As a result, the profile illustration shrinks.

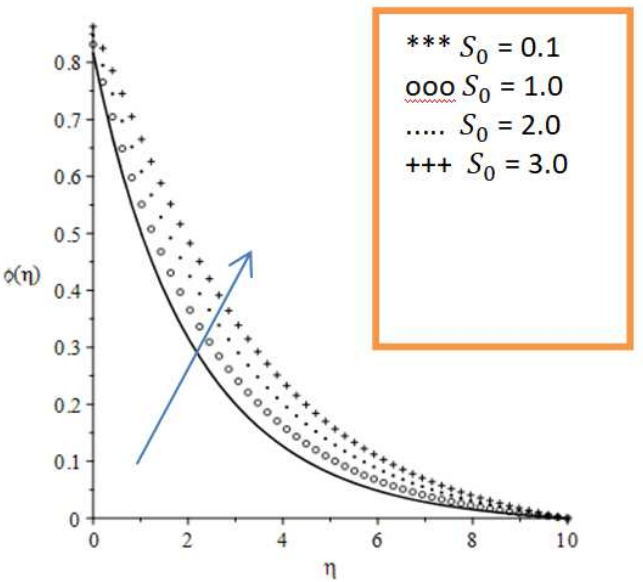

Figure 19: Concentration graph for various values of Soret number.

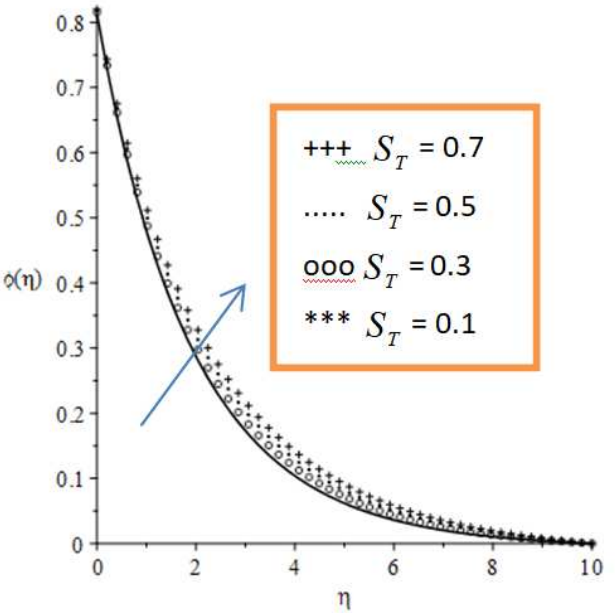

Figure 20: Concentration graph for various values of thermal stratification parameter.

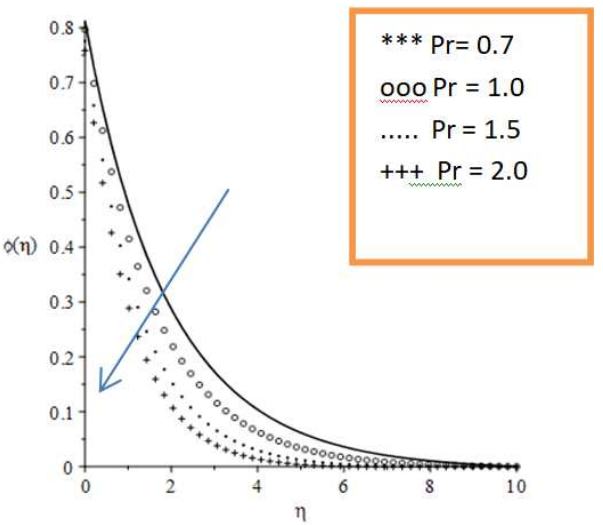

Figure 21: Concentration graph for various values of Prandtl number.

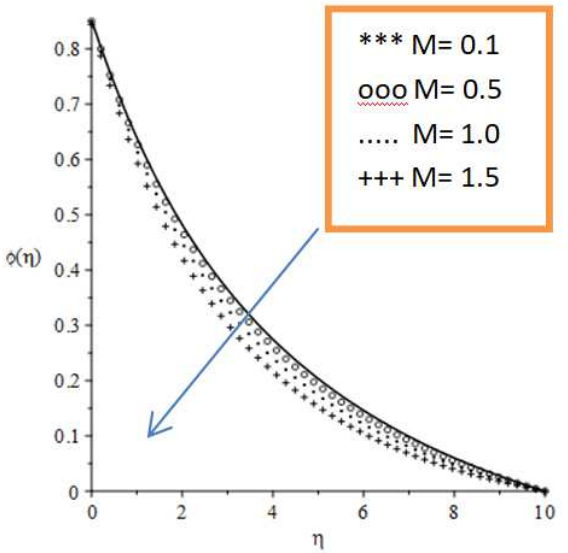

Figure 22: Concentration graph for various values of magnetic field parameter.

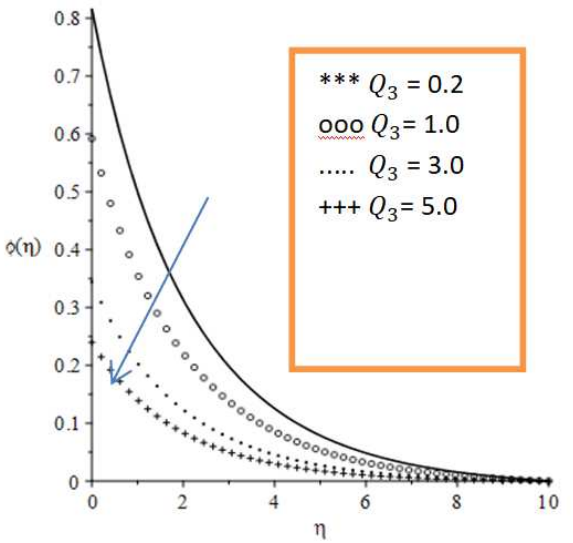

Figure 23: Concentration graph for various values of Solutal slip parameter.

5. Conclusion

The effects of dual stratification on mixed convective electro-magnetohydrodynamic flow over a stretching plate with multiple slips and cross diffusion has been examined in this study. The partial differential equations were converted into nonlinear ordinary differential equations with the aid of similarity analysis. The nonlinear equations were solved using the fourth-order Runge-Kutta method with Newton Raphson shooting technique.

- The skin friction coefficient was enhanced when the suction number, Prandtl number, permeability parameter, Soret number, thermal stratification parameter, thermal slip parameter, magnetic field parameter and buoyancy ratio parameter were increased.
- As the solutal stratification parameter, Soret number, solutal slip parameter, Richardson number, electric field parameter, suction, and Prandtl numbers increased, the heat transfer rate towards the plate surface is increased.
- With the increase in Lewis number, Dufour number, Richardson number, electric field parameter, Brinkmann number, chemical reaction parameter, thermal slip parameter, suction parameter and Prandtl number, the mass transfer rate at the surface increased.
- The momentum boundary layer thickness was increased by solutal stratification parameter, Dufour number, solutal slip parameter, Lewis number, magnetic field parameter, electric field parameter, chemical reaction parameter, Richardson number, and Brinkmann number while the Soret number, Prandtl number, suction parameter and Buoyancy ratio parameter decreased the momentum boundary layer thickness.
- The thermal boundary layer thickness was increased by permeability parameter, magnetic field parameter, Dufour number, Brinkmann number, buoyancy ratio parameter, momentum slip parameter, and Soret number, but the solutal stratification parameter, Lewis number, electric field parameter, solutal slip parameter, chemical reaction parameter, Prandtl number, Richardson number, suction parameter, and thermal slip parameter increased the thickness of the thermal boundary layer.

- The Soret number, buoyancy ratio parameter, thermal slip parameter, permeability parameter, momentum slip parameter, and thermal stratification all enhanced the thickness of the solutal boundary layer.
- The solutal boundary layer thickness was depleted by the magnetic field parameter, Dufour number, Brinkmann number, solutal stratification parameter, electric field parameter, suction parameter, chemical reaction parameter, Richardson number, Prandtl number, solutal slip parameter and Lewis number.

6. Conflict of Interest

The authors declared no conflicts of interest for the current study, authorship, and publication of this paper.

7. Funding

The authors did not receive any financial assistance from anywhere for the publication of this paper.

References

[1] Hayat, T., Waqas, M., Khan, M. I., & Alsaedi, A. (2016). Analysis of thixotropic nanomaterial in a doubly stratified medium considering magnetic field effects. *International Journal of Heat and Mass Transfer*, *102*, 1123-1129. https://doi.org/10.1016/j.ijheatmasstransfer.2016.06.090

[2] Srinivasacharya, D., & Upendar, M. (2013). Effect of double stratification on MHD free convection in a micropolar fluid. *Journal of Egyptian Mathematical Society*, *21*, 370-378. https://doi.org/10.1016/j.joems.2013.02.006

[3] Jian, Y., & Chang, L. (2015). EMHD micropumps under a spatially non-uniform magnetic field. *ATP Advances*, 057121. https://doi.org/10.1063/1.4921085

[4] Yahaya, S. D., & Faisal, S. (2018). Impact of thermal radiation on electrical MHD flow of nanofluid over a nonlinear stretching sheet with variable thickness. *Alexandria Engineering Journal*, *57*, 2187-2197. https://doi.org/10.1016/j.aej.2017.07.007

[5] Besthapy, P., Haq, R., Bandari, S., & Al-Mdallal. (2017). Mixed convection flow of thermally stratified MHD nanofluid over an exponentially stretching surface with viscous dissipation effect. *Journal of Taiwan Institute of Chemical Engineers*, *71*, 307-314. https://doi.org/10.1016/j.jtice.2016.12.034

[6] Mutuku, W. N., & Makinde, O. D. (2017). Double stratification effect on heat and mass

transfer in unsteady MHD nanofluid flow over a flat surface. *Asia Pacific Journal of Computational Engineering*, 4, 2, https://doi.org/10.1186/s40540-017-0021-2

[7] Khashi'ie, N. S., Arifin, N. M., & Hafidzuddin, E. H. (2019). Dual stratified nanofluid flow past a permeable shrinking/stretching sheet using non-Fourier energy model. *Applied Sciences*, *9*, 2124. https://doi.org/10.3390/app9102124

[8] Reddy, P. S., & Chamkha, A. J. (2015). Soret and Dufour effects on unsteady MHD heat and mass transfer from a permeable stretching sheet with thermophoresis and non-uniform heat generation absorption. *Journal of Applied Fluid Mechanics*, *9*(5), 2443-2455. https://doi.org/10.18869/acadpub.jafm.68.236.25171

[9] Dulal, P., Gopinath, M., & Kuppalaplle, V. (2016). Soret and radiative heat and mass transfer of nanofluid over a vertical nonlinear stretching shrinking sheet. *Applied Mathematics and Computation*, *287-288*, 184-200. https://doi.org/10.1016/j.amc.2016.04.037

[10] Gireesha, B. J., Kumar, K. G., Krishnamurthy, M. R., Manjunatha, S., & Rudraswamy, N. G. (2019). Impact of ohmic heating on MHD mixed convection flow of Casson fluid by considering cross diffusion effect. *Nonlinear Engineering*, *8*(1), 380-388. https://doi.org/10.1515/nleng-2017-0144

[11] Gbadeyan, J. A., Oyekunle, T. L., Fasogbon, P. F., & Abubakar, J. U. (2018). Soret and Dufour effects on heat and mass transfer in chemically reacting MHD flow through a wavy channel. *Journal of Taibah University for Science*, *12*(5), 631-651. https://doi.org/10.1080/16583655.2018.1492221

[12] Reddy, B. S. K., Rao, K. V. S. N., & Vijaya, R. B. (2020). Soret and Dufour effect on MHD flow of viscous elastic fluid pass on an infinite vertical stretching sheet. *Heat Transfer*, *49*(4), 2330-2343. https://doi.org/10.1002/htj.21723

[13] Rasool, G., Shafiq, A., & Baleanu, D. (2020). Consequences of Soret-Dufour effects on thermal radiation and binary chemical reaction on Darcy-Forchheimer flow of nanofluids. *Symmetry*, *12*, 1421. https://doi.org/10.3390/sym12091421

[14] Salleh, S. N. A., Bachok, N., Araifin, N. M., & Ali, F. M. (2020). Influence of Soret and Dufour on forced convection flow towards a moving thin needle considering Buongiorno's nanofluid model. *Alexandria Engineering Journal*, *59*(5), 3897-3906. https://doi.org/10.1016/j.aej.2020.06.045

[15] Bouslimi, J., Abdelhafez, M. A., Abd-Alla, A. M., Abo-Dahab, S. M., & Mahmoud, K. H. (2021). MHD mixed convection nanofluid flow over convectively heated nonlinear due to an extending surface with Soret Effect. *Complexity*, vol. 2021, Article ID 5592024, 20 pages. https://doi.org/10.1155/2021/5592024

[16] Turkyilmazoglu, M. (2011). Multiple solutions of heat and mass transfer of MHD slip flow for the viscoelastic fluid over a stretching sheet. *International Journal of Thermal Sciences*, *50*(11), 2264-2276. https://doi.org/10.1016/j.ijthermalsci.2011.05.014

[17] Daniel, Y. S., Azie, Z. A., Ismail, Z., & Salah, F. (2017). Effects of MHD flow of nanofluids over a porous nonlinear stretching/shrinking sheet. *Australian Journal of Mechanical Engineering*, *16*(3), 213-229. https://doi.org/10.1080/14484846.2017.1358844

[18] Khan, S. A., Nie, Y., & Ali, B. (2020). Multiple slip effects on MHD unsteady viscoelastic nanofluid flow over a permeable stretching sheet with radiation using the finite element method. *SN Applied Science*, *2*, 66. https://doi.org/10.1007/s42452-019-1831-3

[19] Khan, S. A., Nie, Y., & Ali, B. E. (2019). Multiple effect MHD axisymmetric buoyant nanofluid flow above a stretching radiation and chemical reaction. *Symmetry*, *11*(9), 1171. https://doi.org/10.3390/sym11091171

[20] Mabood, F., & Shateyi, S. (2019). Multiple slip effect on MHD unsteady flow heat and mass transfer impinging on permeable stretching sheet with radiation. *Modeling and Simulation in Engineering*, vol. 2019, Article ID 3052790, 11 pages. https://doi.org/10.1155/2019/3052790

[21] Wahid, N. S., Hafidzuddin, M. E. H., Arifin, N. M., Turkyilmazoglu, M., & Rahmia, N. A. A. (2020). MHD slip Darcy flow of viscoelastic fluid over a stretching sheet and heat transfer with thermal radiation and viscous dissipation. *CFD Letters*, *12*(1), 1-12.

[22] Abbas, W., Ahmed, M., Megahed, M., Ibrahim, A., Ahmed, A., & Said, M. (2023). Non-Newtonian slippery nanofluid flow due to a stretching sheet through a porous medium with heat generation and thermal slip. *Journal of Nonlinear Mathematical Physics*, https://doi.org/10.1007/s44198-023-00125-5

[23] Ibrahim, W., & Gizewu, T. (2021). Thin film flow of tangent hyperbolic fluid with nonlinear mixed convection flow and entropy generation. *Mathematical Problems in Engineering*, *2021*, 1-16. https://doi.org/10.1155/2021/4836434

[24] Yin, Yu-Hang, Lü, Xing, & Ma, Wen-Xiu. (2022). Bäcklund transformation, exact solutions, and diverse interaction phenomena to a (3+1)-dimensional nonlinear evolution equation. *Nonlinear Dynamics*, *108*, 4181-4194. https://doi.org/10.1007/s11071-021-06531-y

[25] Biswal, M. M., Swain, B. K., Das, M., & Gouranga, C. D. (2022). Heat and mass transfer in MHD stagnation-point flow toward an inclined stretching sheet embedded in a porous medium. *Heat Transfer*, *51*, 4837-4857. https://doi.org/10.1002/htj.22525

[26] Sher Akbar, N., & Mallawi, F. O. (2023). Numerical analysis of non-Newtonian nanofluids under double-diffusive regimes. *Frontiers in Materials*, *9*, 1078467. https://doi.org/10.3389/fmats.2022.1078467

[27] Shehzad, N., Zeeshan, A., Shakeel, M., Ellahi, R., & Sait, S. M. (2022). Effects of magnetohydrodynamics flow on multilayer coatings of Newtonian and non-Newtonian fluids through porous inclined rotating channel. *Coatings*, *12*, 430. https://doi.org/10.3390/coatings12040430

[28] Kumar, D., & Sahu, A. K. (2022). Non-Newtonian fluid flow over a rotating elliptic cylinder in laminar flow regime. *European Journal of Mechanics*, *93*, 117-136. https://doi.org/10.1016/j.euromechflu.2022.01.005

[29] Goyal, M., & Bhargava, R. (2014). Boundary layer flow and heat transfer of viscoelastic nanofluids past a stretching sheet with partial slip conditions. *Applied Nanoscience*, *4*, 761-767.

[30] Wang, C. Y. (1989). Free convection on a vertical stretching surface. *Journal of Applied Mathematics and Mechanics/Zeitschrift für Angewandte Mathematik und Mechanik*, *69*(11), 418-420. https://doi.org/10.1002/zamm.19890691115

[31] Gorla, R. S. R., & Sidawi, I. (1994) Free convection on a vertical stretching surface with suction and blowing. *Applied Scientific Research*, *52*, 247-257. https://doi.org/10.1007/BF00853952